

Matthew S. Gilmore^{1,3}, Jerry M. Straka², and Erik N. Rasmussen^{1,3}

¹ Cooperative Institute for Mesoscale Meteorological Studies, Univ. of Oklahoma, Norman, OK

² School of Meteorology, Univ. of Oklahoma, Norman, OK

³ NOAA/National Severe Storms Laboratory (NSSL), Boulder, CO

1. INTRODUCTION

In order to improve warm season flood forecasting, efforts are underway to couple rainfall output from cloud-scale atmospheric models to hydrological models. However, before such efforts can bear fruit, the variation in rainfall due to the uncertainties inherent in microphysical parameterizations must be assessed. Understanding these microphysical sensitivities is a major focus of the U.S. Weather Research Program (Droegemeier et al. 2000).

Here, we will demonstrate large model sensitivity in rainfall and hailfall due to variations in microphysical input specifications that describe the hail/graupel distribution. The 3-class ice microphysical package used in our study (hereafter, LFO-3) is very similar to that presented by Lin et al. (1983). LFO-3 is a prime candidate for study since Lin et al (1983) schemes are routinely used in forecast models such as the Advanced Regional Prediction Model (Xue et al. 2001) and the Weather Research and Forecasting Model (Michalakes et al. 2000). We hope that our investigation will motivate an exploration of how such uncertainties should be treated in cloud scale and hydrological forecast models.

2. REVIEW OF THE ICE MICROPHYSICS SCHEME

LFO-3 predicts a single moment, bulk mixing ratio, for each precipitating class. The negligibly precipitating particles (cloud ice and cloud water) are mono-dispersed. The faster precipitating particles (rain, snow, and hail/graupel) are defined by inverse-exponential size distributions wherein the most numerous particles (n) are found at the smallest diameter sizes (D).

$$n_x(D) = n_{ox} \exp(-D_x \lambda_x^{-1}) \quad (\text{m}^{-4}), \quad (1)$$

wherein x is r (rain), s (snow), or h (hail). The mean size of each distribution is equal to the slope parameter,

$$\lambda_x = [\rho q_x / (\pi \rho_x n_{ox})]^{1/4} \quad (\text{m}), \quad (2)$$

wherein ρ_x is the species particle density, n_{ox} is the intercept parameter, ρ is the local air density, and q_x is the species mixing ratio. (The total number of particles

at an instant in time can be found using, $n_x = n_{ox} \lambda_x^{-3}$, m^{-3} .) Thus, each distribution is a function of ρ_x and n_{ox} .

Notice that within LFO-3, both hail and graupel are represented by a single category called "hail/graupel". This means that one must artificially choose a constant ρ_h and n_{oh} a priori to represent both types of particles. Herein, hail and graupel are individually defined as those particles in the hail/graupel distribution that are greater than or less than 5 mm, respectively.

3. EXPERIMENTAL DESIGN

The Straka Atmospheric Model (Johnson et al. 1993; Straka and Anderson 1993; Carpenter et al. 1998) is the three-dimensional, non-hydrostatic cloud model used for the simulations. Grid spacing of $\Delta z = 500$ and $\Delta x = \Delta y = 1000$ m are used in a $90 \times 90 \times 22$ km³ domain.

3.1. Initial Conditions

The model is initialized with the idealized temperature and moisture profile described in Weisman and Klemp (1984; hereafter WK84). Environmental CAPE is 2200 J kg⁻¹. The vertical wind shear profile is represented by a half-circle hodograph that traces an arc length of 50 m s⁻¹ over the lowest 5 km AGL. (Results using a 30 m s⁻¹ arc length hodograph are omitted here for the sake of brevity.) Above $z = 5$ km AGL, the wind speed is held constant at the $z = 5$ km value. An axially symmetric thermal bubble with maximum temperature excess of +1°C is used to initiate convection (e.g., Klemp and Wilhelmson 1978).

3.2. Microphysics treatments

The sensitivity experiments were designed by varying the bulk particle density and intercept parameter constants for the hail/graupel category. There are numerous in situ observations motivating these experiments. Graupel density varies from 50 to 890 kg m⁻³ and hail density varies from 700 to 900 kg m⁻³ in observed storms (Pruppacher and Klett 1978). Also, n_{oh} varies from 10^3 to 10^5 for hail and is as high as 10^{10} for graupel (Dennis et al. 1971; Federer and Waldvogel 1975; Spahn 1976; Knight et al. 1982). Combinations over a range of the observed values were chosen and are shown in Table 1. In addition, a warm-rain

* Corresponding author address: Matthew S. Gilmore, NOAA/NSSL, 325 Broadway N/C/MRD, Boulder, CO 80305-3328; e-mail: Matthew.Gilmore@nssl.noaa.gov

simulation (ice processes turned off; hereafter referred to as WR) was performed for reference.

The N3p9 and N8p4 cases allow the greatest number of hail and graupel particles, respectively, with other cases having intermediate amounts (Fig. 1a). Mass is distributed over a smaller range and is weighted toward the smallest-sized particles for the N8p4 case (not shown). Both a smaller particle density and a larger intercept parameter conspire to give a smaller mass-weighted mean terminal fall velocity (V_t) over all ranges of water content (Fig. 1b).

Table 1. Parameters used to define the inverse-exponential distributions for the hail/graupel category. The rain and snow parameters are held constant. Rain and snow have particle densities of 100 and 1000 kg m^{-3} and intercepts of 8×10^6 and $3 \times 10^6 \text{ m}^{-4}$, respectively. The treatments are labeled as $Napb$ wherein a is the exponent in the slope intercept parameter, $4 \times 10^a \text{ m}^{-4}$, and b is the first digit in particle density, $b00 \text{ kg m}^{-3}$. N5p4 and N7p4 cases were also performed but are omitted here due to redundancy.

Simulation	n_{oh} (m^{-4})	Bulk Particle Density (kg m^{-3})
N3p9	4×10^3	900
N4p9	4×10^4	900
N5p9	4×10^5	900
N4p4	4×10^4	400
N6p4	4×10^6	400
N8p4	4×10^8	400

4. RESULTS AND DISCUSSION

Compared to the N3p9 storms, the N8p4 storms have stronger and wider updrafts, warmer minimum temperatures in the low-level outflow, smaller gradients in precipitation, and more precipitation spreading farther downstream (Fig. 2). The N8p4 right-moving supercell also experiences less southward movement by approximately 15 km (Fig. 2b); apparently due to a weaker cold pool. Evolutions for other cases fall between these two.

The maximum updraft speed increases gradually from a hail-weighted distribution to a graupel-weighted distribution (Fig 3). This is due to increasing latent heat release and a warmer updraft above $z = 4 \text{ km AGL}$ (Fig. 4a). As one marches from N3p9 to N8p4, low-level downdrafts weaken (not shown), the minimum temperature within the cold pool warms ($z \leq 1 \text{ km AGL}$ in Fig. 4b), and the minimum temperature decreases near the melting level and rises in altitude ($2 \leq z \leq 4 \text{ km AGL}$ in Fig. 4b). In addition, the amount of time-average rain decreases at low levels while the amount of graupel/hail at upper levels (and its prevalent altitude) increases (Fig. 5a). The average amounts of snow,

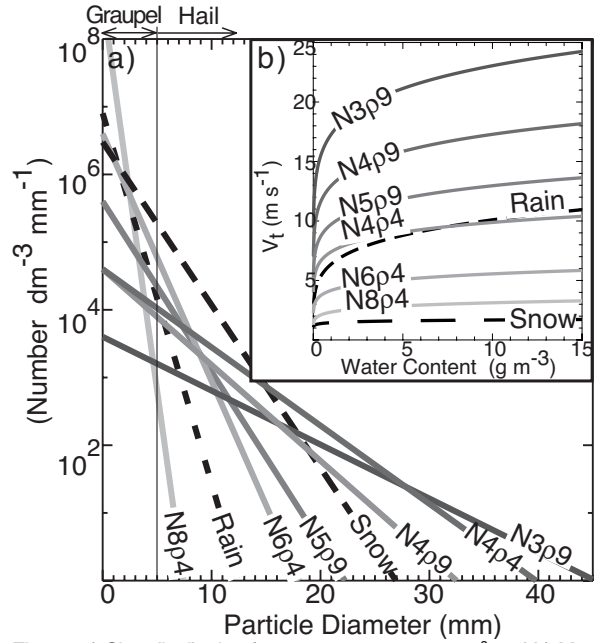


Fig. 1. a) Size distribution for water content 10 g m^{-3} and b) Mass-weighted mean terminal fall velocity (V_t) as a function of water content for each species ($z=4.5 \text{ km AGL}$).

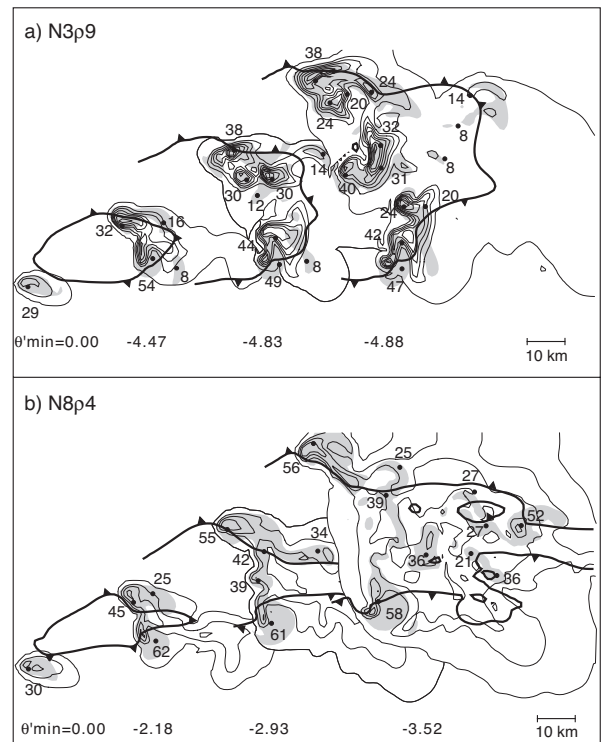


Fig. 2. Evolution in midlevel storm structure depicted at 30, 60, 90, and 120 min for cases a) N3p9 and b) N8p4. Total precipitation mixing ratio at $z=4.75 \text{ km AGL}$ is contoured at 2 g kg^{-1} intervals beginning at 0.1 g kg^{-1} . Regions of updraft $> 5 \text{ m s}^{-1}$ at $z = 4.75 \text{ km AGL}$ are shaded with the updraft maxima located by dots and labeled in m s^{-1} . The surface gust front (-0.5°C perturbation potential temperature, θ') is denoted by a thick barbed line. The surface θ' ($^\circ\text{C}$) minimum is also shown.

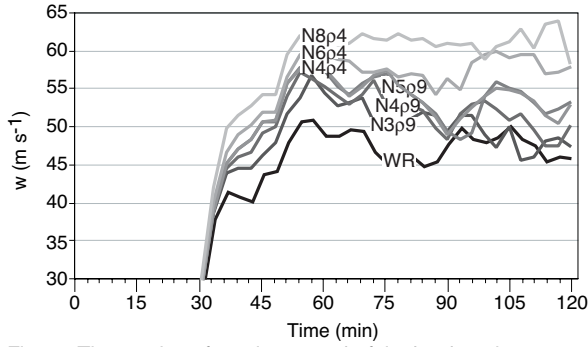


Fig. 3. Time series of maximum updraft in the domain.

cloud ice, cloud water, and rain ($z > 5$ km) also decrease as one marches from N3p9 to N8p4 (Fig. 5).

These kinematical and microphysical changes occur due to changes in the hail/graupel V_i and those growth rate equations that are a function of hail/graupel ρ_h and n_{oh} . The deposition rate of hail/graupel and all accretion rates by hail/graupel are larger in N8p4 versus N3p9 (Fig. 6). This helps explain the warmer and faster updrafts in the graupel-weighted cases. The increased rate by which hail/graupel accretes snow, cloud ice, cloud water, and rain also explains their reduced amounts in the graupel-weighted cases (Fig. 5).

However, the increased sublimation and melting rates outside the updraft, along with much slower V_i , results in much less precipitation reaching ground in N8p4 compared to N3p9 (27 Tg versus 78 Tg; Table 2). Also, the maximum precipitation depth accumulation in N8p4 is about three times less than N3p9 (21 versus 57 mm; not shown).

Additional experiments (not shown here) demonstrate that the model's accumulated precipitation is less sensitive to, but in the same direction as, equivalent magnitude changes in the intercept

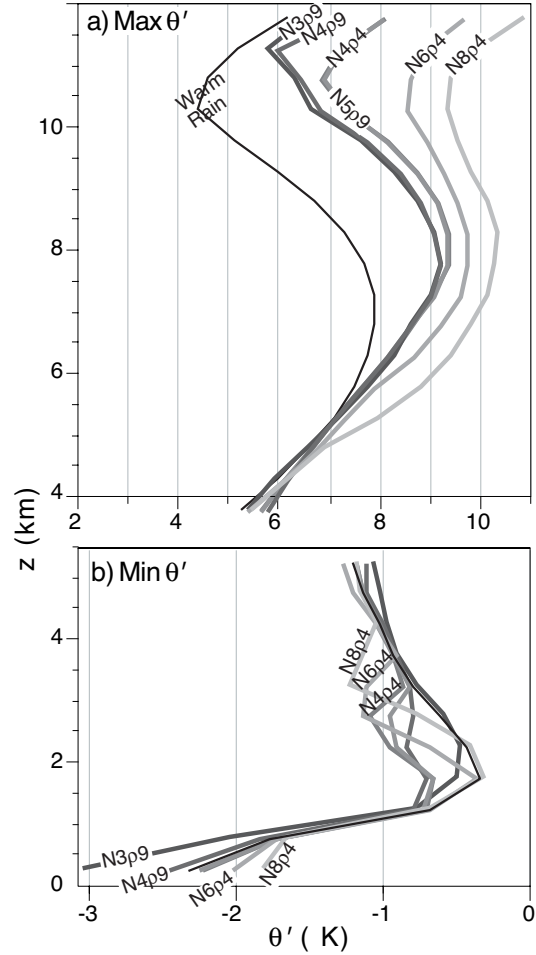


Fig. 4. Time-averaged altitude profiles of a) maximum domain θ' and b) minimum domain θ' for the 6 ice-microphysical parameterizations and the warm rain parameterization (thin black line). The average was computed using model data sampled every 3 minutes from $t=0$ to $t=120$ minutes.

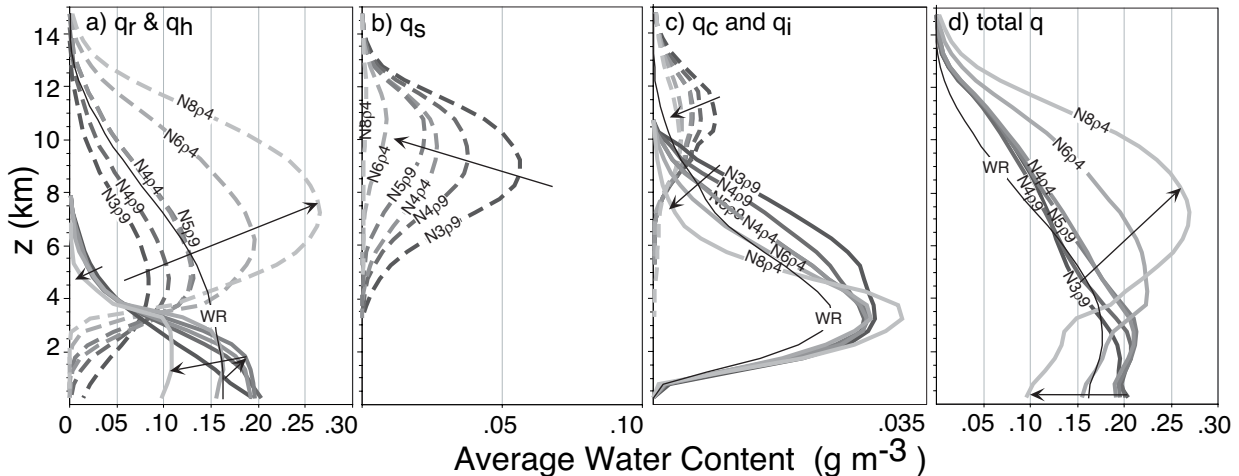


Fig. 5. Plots of temporally- and spatially- averaged water content (g m^{-3}) as a function of altitude for the 7 cases in the study. Cases are shown in terms of a) rain and hail/graupel, b) snow, c) cloud water and cloud ice, and d) total water. Temporal averaging was performed upon data output with 3 min frequency from $t=0$ to $t=120$ min. Spatial averaging was performed horizontally with every point in the 90×90 km grid. Arrows show the direction of change from N3p9 to N8p4.

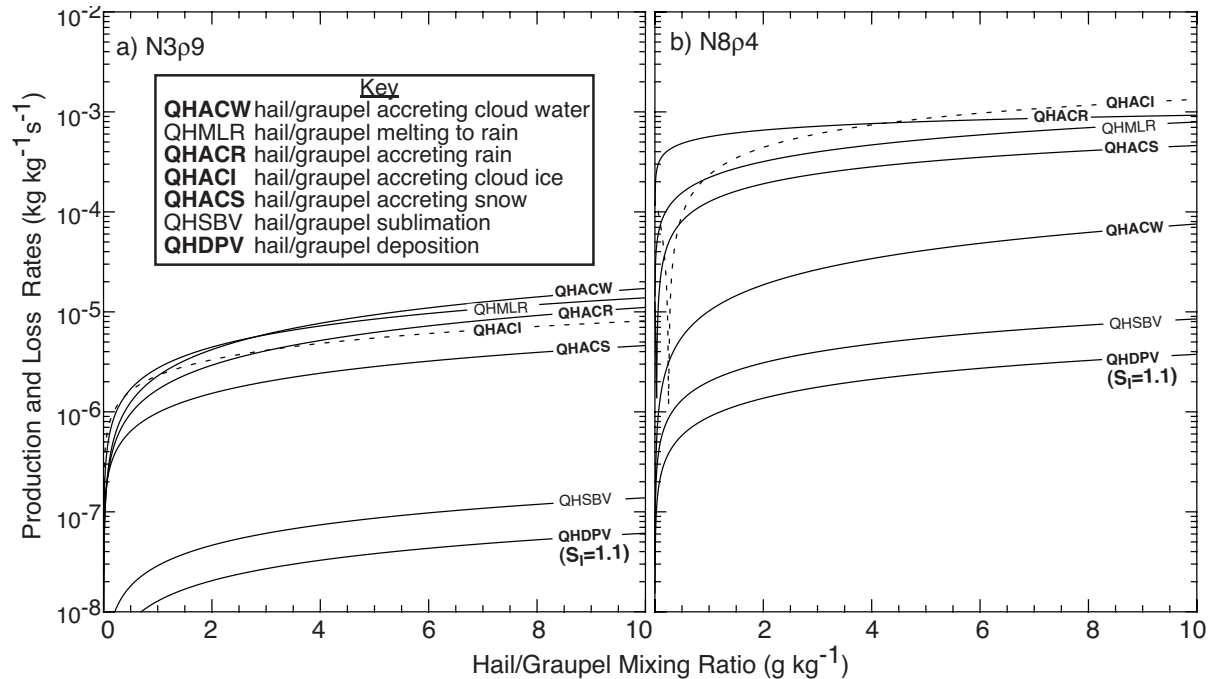


Fig. 6. Production and loss rates as a function of hail/graupel mixing ratio for $z = 6.25$ km altitude (except for qhmlr, valid for $z = 3$ km AGL) in the WK84 environmental sounding for cases a) N3p9 and b) N8p4. Only those rates that change with hail/graupel intercept and/or density are shown. Those processes labeled with non-bold and bold lettering refer to sinks and sources for hail/graupel, respectively. Accretion rates (qhacw, qhaci, qhacr, and qhacs) were computed assuming a mixing ratio of 1 g kg^{-1} for the accreted particles. For hail/graupel deposition (qhdpv), a 10% supersaturation with respect to ice was assumed. The dotted line for qhaci indicates that the production rate was hypothetical since cloud ice of 1 g kg^{-1} was not present in any of the simulations at the reference altitude of $z = 6.25$ km AGL (however, that amount and greater was found at a higher altitude).

Table 2. Ground-accumulated precipitation mass by $t = 2$ hours.

Simulation	Accumulated Mass (teragrams)		
	Total	Rain	Hail
N3p9	77.59	67.49	10.096
N4p9	71.10	70.53	0.569
N5p9	66.63	66.61	0.015
N4p4	64.86	64.83	0.035
Warm Rain	56.17	56.17	0
N6p4	48.64	48.64	17×10^{-6}
N8p4	27.21	27.21	~ 0

parameter for rain or snow.

We warn the reader that the large differences in accumulated precipitation between cases might result from the fact that large hail is more prolific in supercells. A previous study of simulated tropical squall lines (albeit, with a smaller range of intercepts) did not show such large precipitation-fall differences between cases (McCumber et al. 1991). However, we have also found a factor of three difference in accumulated precipitation when our experiments were repeated with weaker shear (30 m s^{-1} arc length hodograph) and therefore the microphysical uncertainty cannot be discounted.

The reader may wonder whether the N8p4 case bears any resemblance to the so-called "low-precipitation (LP) supercell" (Moller et al. 1994). Too few in situ observations exist to evaluate whether actual LP storms store most of their water mass in

graupel versus another ice species. Also, N8p4 is incapable of simulating large hailstones that are often observed with LP supercells. This limitation arises because hail and graupel in LFO-3 are represented within a single species that has fixed ρ_h and n_{oh} .

We have shown that the precipitation accumulation beneath deep convective storms simulated with LFO-3 microphysics can vary by a factor of three due to uncertainties in specifying the hail/graupel distribution. Therefore, the utility of this scheme in warm season cloud-scale precipitation forecasting is questionable. However, understanding these sensitivities is an important first step in motivating the use of more sophisticated ice microphysics schemes that do not require arbitrary prescription of hail/graupel intercept and density.

5. ACKNOWLEDGMENTS

This research was supported by the National Science Foundation under grants ATM-0003869 and ATM-9617318. Partial funding for this research was provided by the NSSL under NOAA-OU Cooperative Agreement #NA67RJ0150.

6. REFERENCES

References are available upon request.